Improving the performances of current optical interferometers & future designs
Proceedings of Haute Provence Observatory Colloquium (23-27 September 2013)
Edited by L. Arnold, H. Le Coroller & J. Surdej

Linearized Model of an Actively Controlled Cable for a Carlina Diluted Telescope

Torben Andersen[1], Hervé Le Coroller[2], Mette O.-Petersen[1] & Julien Dejonghe[3]

[1] *Lund Observatory, Box 43, SE-221 00 Lund, Sweden*

[2] *Observatoire de Haute Provence, F-04870 St Michel l'Observatoire, France*

[3] *Laboratoire Lagrange - UMR 7293, Observatoire de la Côte d'Azur, B.P. 4229, F-06304 NICE Cedex 4, France*

Abstract. The Carlina thinned pupil telescope has a focal unit ("gondola") suspended by cables over the primary mirror. To predict the structural behavior of the gondola system, a simulation building block of a single cable is needed. A preloaded cable is a strongly non-linear system and can be modeled either with partial differential equations or non-linear finite elements. Using the latter, we set up an iteration procedure for determination of the static cable form and we formulate the necessary second-order differential equations for such a model. We convert them to a set of first-order differential equations (an "ABCD"-model). Symmetrical in-plane eigenmodes and "axial" eigenmodes are the only eigenmodes that play a role in practice for a taut cable. Using the model and a generic suspension, a parameter study is made to find the influence of various design parameters. We conclude that the cable should be as stiff and thick as practically possible with a fairly high preload. Steel or Aramid are suitable materials. Further, placing the cable winches on the gondola and not on the ground does not provide significant advantages. Finally, it seems that use of reaction-wheels and/or reaction-masses will make the way for more accurate control of the gondola position under wind load. An adaptive stage with tip/tilt/piston correction for sub-apertures together with a focus and guiding system for freezing the fringes must also be studied.

1. Introduction

The planned Carlina telescope (Le Coroller et al. 2012, Dejonghe et al. 2014) will have a gondola with focal plane optics suspended in a cable net over the primary mirror. The position of the gondola must be controlled accurately by a dynamical control system with cable winches. To model this system, a dynamical, state-space model of a guy wire is needed. We here present such a model and some test runs with conclusions related to choice of design parameters.

Most structures can be adequately described by linear models. However, in some cases non-linear techniques are necessary. Two types of non-linearities are common: Material and geometric non-linearities. Creeping of steel is a well-known example of a material non-linearity. Geometric non-linearities arise when the deformation of a structure is so large that changes of the geometry of the structure play a significant role for the load path in the structure. A wire is a geometrically non-linear system because the system geometry changes due to gravity loads and external forces.

Modeling of suspended cables is difficult but of high interest due to important applications, such as suspension bridges, wire roof structures, guyed antenna masts, semi-submersible drilling rigs, and electrical transmission lines.

The problem related to gondola control for the Carlina is that many simulation and control tools are linear, so it is of interest to establish a linear state-space model of the cable performance. The approach is then to first establish a non-linear model to determine the operating point of the cable and then a linear model describing performance around the operating point.

Two types of models can be used to describe cables, either based on partial differential equations (Irvine 1981, Starossek 1994) or on a finite element representation (Henghold & Russell 1976, Ozdemir 1979, Desai et al. 1988, Tibert 1999, Talvik 2001). In a previous publication (Enmark et al. 2011), a model based upon partial differential equations was used. We here present a cable model based upon a finite element approach (largely following Tibert 1999) and draw some conclusions for the choice of design parameters.

In Section 2, we present the equations for a finite cable element, and in Section 3 we show the algorithms for determination of the static form a of suspended cable. Then, in Section 4, we set up a linear, dynamic model of a cable, valid for small excursions around the operating point, and in Section 5 we comment on the nature of the wind loads. Finally, a generic gondola suspension model is formulated in Section 6 for evaluation of design parameter sensitivity, together with a concluding discussion in Section 7. Through the paper, we illustrate the approach by an example of a cable similar to the ones used for the Carlina.

2. Single Element

A finite element model of a cable can be formed as shown in Fig. 1 for a horizontal wire. The cable is divided into a number of elements and corresponding masses are assigned to the nodes between the elements. Under the influence of gravity and preload, the wire assumes a certain form. With modest preloads this is the well-known catenary, whereas it resembles a parabola, when the preload is high. Each node has three translational degrees of freedom.

Figure 2 shows part of a finite element model of a wire for the static case. If the node in B for some reason is displaced from the equilibrium position to position B', two different effects together tend to restore equilibrium. Firstly, elements AB and BC are stretched so in addition to the preload, axial, *elastic* forces turn up. Secondly, due to the displacement of node B, the two preload forces in elements AB and BC change direction, leading to a *geometric* force component ΔF_B that tends to move the node back from B' to its equilibrium position in B. The two effects can be dealt with separately by use of elastic and geometric stiffness matrices, respectively.

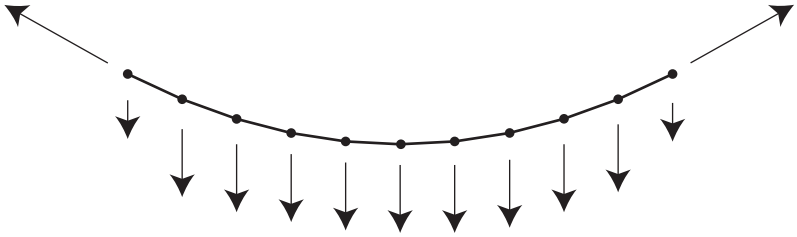

Figure 1.: *Subdivision of a cable into finite elements connected at nodes.*

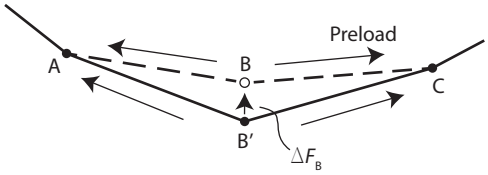

Figure 2.: *Displacing node B to B' creates a geometric restoring force.*

Different cable elements are described in the literature (Gambhir & Barrington De V. Batchelor 1977, Jayaraman & Knudson 1981, Ahmadi-Kashani 1983, Tibert 1999, Ren et al. 2008). For highly preloaded cables, rectilinear elements suffice, whereas curved elements are useful for less preloaded cables. Due to the high preload, simple rectilinear elements (Tibert 1999, Levy & Spillers 2003) can be used for the Carlina.

A rectilinear cable element in 3D Cartesian space (x, y, z) between nodes number i and j is shown in Fig. 3. We first wish to form the elastic stiffness submatrix from which the elastic end node force increments at node i can be determined by multiplication by a displacement vector for the same node. Letting $\mathbf{n_{ij}}$ denote a unit vector directed from node i to node j it can relatively easily be shown (Levy & Spillers 2003) that the elastic stiffness submatrix, $\mathbf{K}_{\mathrm{Ei}}$, for node i is

$$\mathbf{K}_{\mathrm{Ei}} = \frac{AE}{L} \times \mathbf{n}_{\mathrm{ij}} \mathbf{n}_{\mathrm{ij}}^{\mathrm{T}}$$

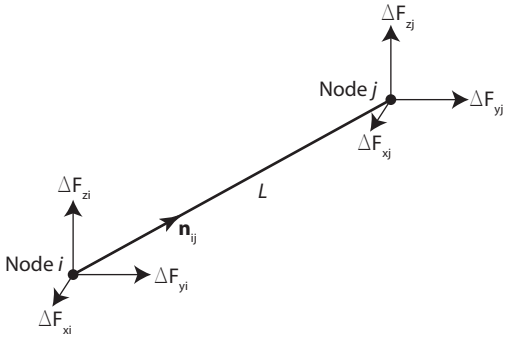

Figure 3.: *An element connecting nodes i and j in 3D space. End point forces in a global coordinate system are shown.*

where the symbols are defined in Table 1 together with some values used in the example of this note. The operator "$\circ^{\mathrm{T}}$" transposes a matrix. For reasons of symmetry, the full, elastic stiffness matrix for the element then is

$$\mathbf{K}_{\mathrm{E}} = \begin{bmatrix} \mathbf{K}_{\mathrm{Ei}} & -\mathbf{K}_{\mathrm{Ei}} \\ -\mathbf{K}_{\mathrm{Ei}} & \mathbf{K}_{\mathrm{Ei}} \end{bmatrix}$$

Table 1.: *Nomenclature with values used in the example.*

	Definition	Example
F_{i}	Axial force in element i	
F	Cable preload	1344 N
A	Cable cross section	2.69 mm^2
E	Modulus of elasticity	7.03×10^{10}N/m^2
l	Cable chord length	185.8 m
L	Length of element	4.61 m
ρ	Mass density	1440 kg/m^3
θ	Cable inclination angle	19$^{\mathrm{o}}$ or 0$^{\mathrm{o}}$
g	Gravity acceleration	9.81 m/s^2
$(x_{\mathrm{i}}, y_{\mathrm{i}}, z_{\mathrm{i}})$	Coordinates of end point i	(0 m, 0 m, 0 m)
$(x_{\mathrm{j}}, y_{\mathrm{j}}, z_{\mathrm{j}})$	Coordinates of end point j	(175.68 m, 0 m, 60.49 m) or (185.8 m, 0 m, 0 m)

Similarly, the geometric stiffness submatrix for the element at node i can be formed (Levy & Spillers 2003). It is

$$\mathbf{K}_{Gi} = \frac{F_i}{L}\left(\mathbf{I} - \mathbf{n_{ij}}\mathbf{n_{ij}^{\mathrm{T}}}\right)$$

where $\mathbf{I}$ is the identity matrix, F_i the axial force in the element and L the length of the element. As expected, the geometric stiffness matrix depends on the load conditions, leading to a nonlinear model. The full, geometric stiffness matrix then is

$$\mathbf{K}_{\mathrm{G}} = \begin{bmatrix} \mathbf{K}_{\mathrm{Gi}} & -\mathbf{K}_{\mathrm{Gi}} \\ -\mathbf{K}_{\mathrm{Gi}} & \mathbf{K}_{\mathrm{Gi}} \end{bmatrix}$$

and the end node force increments (see Fig. 3) for the element are

$$\begin{Bmatrix} \Delta F_{\mathrm{xi}} \\ \Delta F_{\mathrm{yi}} \\ \Delta F_{\mathrm{zi}} \\ \Delta F_{\mathrm{xj}} \\ \Delta F_{\mathrm{yj}} \\ \Delta F_{\mathrm{zj}} \end{Bmatrix} = (\mathbf{K}_{\mathrm{E}} + \mathbf{K}_{\mathrm{G}}) \begin{Bmatrix} \Delta x_{\mathrm{i}} \\ \Delta y_{\mathrm{i}} \\ \Delta z_{\mathrm{i}} \\ \Delta x_{\mathrm{j}} \\ \Delta y_{\mathrm{j}} \\ \Delta z_{\mathrm{j}} \end{Bmatrix}$$

where $\{\Delta x_{\mathrm{i}}, \Delta y_{\mathrm{i}}, \Delta z_{\mathrm{i}}, \Delta x_{\mathrm{j}}, \Delta y_{\mathrm{j}}, \Delta z_{\mathrm{j}}\}^{\mathrm{T}}$ are the node displacements in directions x, y, and z for nodes i and j with respect to the position at which the stiffness matrices were evaluated.

The matrix $\mathbf{K} = \mathbf{K}_{\mathrm{E}} + \mathbf{K}_{\mathrm{G}}$ is the *tangent stiffness matrix* that describes cable element performance in the vicinity of the node locations at which it was evaluated.

The mass matrix can be formed by simply lumping the mass of the cable to the two end nodes. The mass matrix for a single element then is

$$\mathbf{M} = \frac{1}{2} AL\rho\mathbf{I}$$

3. Cable Static Form

3.1 Approximate Static Form

A cable fixed in the ends and loaded by gravity is taken as taut if the maximum gravity deflection of the cable from its chord is less than about 1/8 of the chord length. Based upon partial differential equations, it is shown by Irvine (1999) that the static gravity deflection for a taut cable is nearly parabolic. For a horizontal cable oriented along the x-axis, the gravity deflection is

$$z = -\frac{\rho A g l^2}{2F}\left(\frac{x - x_1}{l}\left(1 - \frac{x - x_1}{l}\right)\right) \tag{1}$$

where x_1 is the x-coordinate of the first end point of the cable and F the tension force in the cable (taken to be uniform over the length of the cable). For inclined cables, the same expression applies when the gravity vector is scaled appropriately.

For more complex cable networks one may instead use the *force density* method (Schek 1974) which gives a linear set of equations under the assumption that the force per length unit is known. This is a valid approximation for some complex structures.

3.2 Iterative Static Solution

The solution to the static problem dealt with above is only approximate. In the following, an approach for a more exact determination of the static equilibrium form under the influence of gravity and preload is presented. For this, an iterative procedure is necessary.

We first combine all degrees of freedom of the cable into a single global vector. The assumed equilibrium coordinate vector, $\mathbf{u}$, is

$$\mathbf{u} = \left\{x_1, y_1, z_1, x_2, y_2, z_2, \ldots, x_{(\mathrm{n_e}+1)}, y_{(\mathrm{n_e}+1)}, z_{(\mathrm{n_e}+1)}\right\}^{\mathrm{T}}$$

where x_{i}, y_{i}, and z_{i} are the coordinates of node i and n_{e} the number of elements used. This is the first estimate used for the iteration. A good starting point is the node locations found in Sect. 3.1 using an approximate tension force. It is our objective to arrive at a more precise version of this vector. A global vector, $\Delta\mathbf{u}$, with the excursions from the equilibrium is defined as

$$\Delta\mathbf{u} = \left\{\Delta x_1, \Delta y_1, \Delta z_1, \Delta x_2, \Delta y_2, \ldots, \Delta x_{(\mathrm{n_e}+1)}, \Delta y_{(\mathrm{n_e}+1)}, \Delta z_{(\mathrm{n_e}+1)}\right\}^{\mathrm{T}}$$

where Δx_{i}, Δy_{i}, and Δz_{i} are displacements from the assumed equilibrium for node i.

Next, we assemble the global elastic and geometric stiffness matrices, and the global mass matrix, using the expressions for a single element of Sect. 2., and we do this for the node locations defined by $\mathbf{u}$. We here denominate the global elastic matrix by $\mathbf{K}_{\mathrm{E}}$ and get:

$$\mathbf{K}_{\mathrm{E}} = \begin{bmatrix} \mathbf{K}_{\mathrm{E1}} & -\mathbf{K}_{\mathrm{E1}} & & & & & \\ -\mathbf{K}_{\mathrm{E1}} & \mathbf{K}_{\mathrm{E1}}+\mathbf{K}_{\mathrm{E2}} & -\mathbf{K}_{\mathrm{E2}} & & & & \\ & & \ddots & & & & \\ & & -\mathbf{K}_{\mathrm{E(i-1)}} & \mathbf{K}_{\mathrm{E(i-1)}}+\mathbf{K}_{\mathrm{Ei}} & -\mathbf{K}_{\mathrm{Ei}} & & \\ & & & \ddots & & & \\ & & & -\mathbf{K}_{\mathrm{E(n_e-1)}} & \mathbf{K}_{\mathrm{E(n_e-1)}}+\mathbf{K}_{\mathrm{En_e}} & -\mathbf{K}_{\mathrm{En_e}} & \\ & & & & -\mathbf{K}_{\mathrm{En_e}} & \mathbf{K}_{\mathrm{En_e}} & \end{bmatrix}$$

Elements not shown are zero. A similar expression holds for the global geometric stiffness matrix, which we here call $\mathbf{K}_{\mathrm{G}}$. The global mass matrix, which we now call $\mathbf{M}$, simply is

$$\mathbf{M} = \begin{bmatrix} \frac{1}{2}Al\rho & & & & \\ & Al\rho & & & \\ & & \ddots & & \\ & & & Al\rho & \\ & & & & \frac{1}{2}Al\rho \end{bmatrix}$$

The stiffness and mass matrices are $\mathbb{R}^{3(n_e+1)\times 3(n_e+1)}$, sparse, and symmetrical.

For determination of the equilibrium form by iteration we assume that the end points are constrained. Later, when the equilibrium form is known, we will account for displacements of the end points. To constrain the end points, we remove the first and last three rows and columns from the global stiffness matrices (Andersen & Enmark 2011) which we then denote $\mathbf{K}'_{\mathrm{E}}$, and $\mathbf{K}'_{\mathrm{G}}$. Also, for the moment we disregard the degrees of freedom for the end points from the displacement vectors, which we then call $\mathbf{u}'$ and $\Delta\mathbf{u}'$.

We compute the gravity load vector for the inner nodes

$$\mathbf{f}'_g = \mathbf{M}' \{g_{x2}, g_{y2}, g_{z2}, \ldots, g_{xn_e}, g_{yn_e}, g_{zn_e}\}^{\mathrm{T}}$$

where g_{xi}, g_{yi}, and g_{zi} are the components of the i'th gravity vector and $\mathbf{f}'_g \in \mathbb{R}^{3(n_e-1)\times 1}$. Obviously other static forces, such as point loads, may also be added here.

To determine the element forces on the nodes, we determine a vector from the first node of element i to the second node:

$$\mathbf{r}_{\mathrm{i}} = \{x_{\mathrm{i}} - x_{\mathrm{i+1}}, y_{\mathrm{i}} - y_{\mathrm{i+1}}, z_{\mathrm{i}} - z_{\mathrm{i+1}}\}^{\mathrm{T}}$$

The length of the element is $\|\mathbf{r}_{\mathrm{i}}\|$ and a unit vector with the same orientation is

$$\mathbf{n}_{\mathrm{i}} = \mathbf{r}_{\mathrm{i}} / \|\mathbf{r}_{\mathrm{i}}\|$$

The force vector on inner node i ($2 \leq i \leq n_\mathrm{e}$) is

$$\mathbf{f}_i = AE\left(\frac{\|\mathbf{r}_\mathrm{i}\| - l_0}{l_0}\mathbf{n}_\mathrm{i} - \frac{\|\mathbf{r}_\mathrm{i+1}\| - l_0}{l_0}\mathbf{n}_\mathrm{i+1}\right)$$

where l_0 is the length of the unloaded element. The global inner force vector $\mathbf{f}'_e \in \mathbb{R}^{3(n_\mathrm{e}-1)\times 1}$ then is

$$\mathbf{f}'_e = \left\{f_{x2}, f_{y2}, f_{z2}, \ldots, f_{x(n_\mathrm{e}-1)}, f_{y(n_\mathrm{e}-1)}, f_{z(n_\mathrm{e}-1)}\right\}^\mathrm{T}$$

When in equilibrium, $\mathbf{f}'_\mathbf{g}$ and $\mathbf{f}'_\mathbf{e}$ will outbalance each other. When not in equilibrium, the unbalance is

$$\Delta\mathbf{f}' = \mathbf{f}'_g - \mathbf{f}'_e$$

A correction to the estimated inner node coordinates can be found using a combination of the elastic and geometric stiffness matrices:

$$\left(\mathbf{K}'_\mathrm{E} + \mathbf{K}'_\mathrm{G}\right)\Delta\mathbf{u}' = \Delta\mathbf{f}'$$

The equation must be solved for $\Delta\mathbf{u}'$. Using the assignment symbol ":=", the new estimate for $\mathbf{u}'$ then is:

$$\mathbf{u}' := \mathbf{u}' + \Delta\mathbf{u}'$$

with which the iteration can recommence. A stop criterion can be formed by monitoring the relative error

$$\epsilon = \frac{\|\Delta\mathbf{f}'\|}{\|\mathbf{f}'_\mathbf{g}\|}$$

and then interrupt the iteration when $\epsilon < \epsilon_0$, where ϵ_0 is in the range 0.001-0.1. It is possible to reduce computation time by only recalculating the stiffness matrices at certain intervals. Near the end of the iteration, the stiffness matrices only change little. However, for the present application, calculation times are generally small on multithreaded work stations.

Using the iteration procedure described, as an example, the form of the cable defined in Table 1 is determined. The model has 40 elements. The cable is assumed to be horizontal for better illustration. The form depends on the unloaded length of the cable, which was selected as 184.4883 m (the chord length is 185.8 m). The sag in the middle was found to be 0.1210 m and the preload 1344 N. Using Irvine's formula (Irvine 1999) with the same preload of 1344 N a value of 0.1219 m is obtained, in good agreement with the result from our model.

In the vicinity of the equilibrium form, the cable model may be taken as linear. The static deflection relative to the equilibrium form for any small static load may then be determined from the linear equation

$$\left(\mathbf{K}'_\mathrm{E} + \mathbf{K}'_\mathrm{G}\right)\Delta\mathbf{u}' = \Delta\mathbf{f}'$$

As an example, Fig. 4 depicts the incremental form change of the same cable used in the example above with gravity load and an additional downward force of 1 N at distance of 139.35 m from the left cable support.

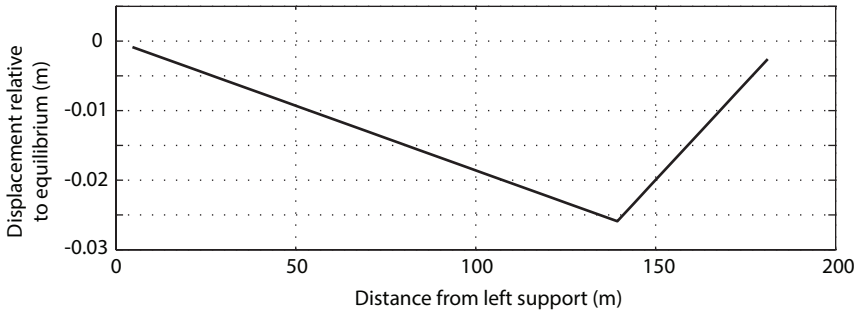

Figure 4.: *Example showing static deflection relative to the equilibrium form due to a downward force of 1 N at a distance 139.35 m from the left support. The two deflection curves seem to be straight lines but that is not exactly the case.*

4. Cable Dynamics

4.1 Dynamical Finite Element Model

Based on the finite element model formulated in Sect. 2., it is relatively easy to set up a dynamical model of the cable. The model can be formed for the case with fixed end points or with free end points. Using the approach described in Andersen & Enmark (2011), the latter model becomes

$$\mathbf{M}\Delta\ddot{\mathbf{u}} + \mathbf{E}\Delta\dot{\mathbf{u}} + \mathbf{K}\Delta\mathbf{u} = \Delta\mathbf{f} \tag{2}$$

Here, $\mathbf{E}$ is a damping matrix. Using standard solvers, the eigenvalues and eigenvectors can be determined (Andersen & Enmark 2011) from

$$\mathbf{K}\boldsymbol{\Psi} = \mathbf{M}\boldsymbol{\Psi}\boldsymbol{\Omega}^{\mathbf{2}}$$

The columns of $\boldsymbol{\Psi}$ are the eigenvectors, the diagonal matrix $\boldsymbol{\Omega}^2$ holds the eigenvalues along the diagonal, and $\boldsymbol{\Omega}$ the eigenfrequencies. By replacing $\mathbf{M}$ with $\mathbf{M}'$, $\mathbf{K}$ with $\mathbf{K}'$, and $\Delta\mathbf{u}$ with $\Delta\mathbf{u}'$, these equations are also valid for the case where the end points are constrained. We call the corresponding matrices of $\boldsymbol{\Psi}$ and $\boldsymbol{\Omega}$ for $\boldsymbol{\Psi}'$ and $\boldsymbol{\Omega}'$.

Using the approach, the eigenmodes and eigenfrequencies for the cable of the previous example can be determined. There are two types of eigenmodes, vertical (in-plane) and lateral (out-of-plane), which again can be subdivided into symmetrical and anti-symmetrical eigenmodes. Figure 5 shows low-order in-plane eigenmodes determined for a cable with the characteristics shown in Table 1. For plotting, the eigenmodes have been scaled to a peak displacement of 0.1 m and are shown superimposed on top of the static deflection curve. Table 2 lists the nature of some more important eigenmodes. High-order eigenmodes are not shown because they are generally not important for control system design and wind load studies. Also the model tends to be inaccurate at higher eigenfrequencies. For studies of the effect of flutter (wind-coupled transverse cable vibrations), a finite-element model with many elements would be needed to model high-order eigenmodes accurately.

For the axial eigenmodes, the cable vibrates with a movement along the "axis" of the cable. These modes resemble that of an air column in an organ pipe

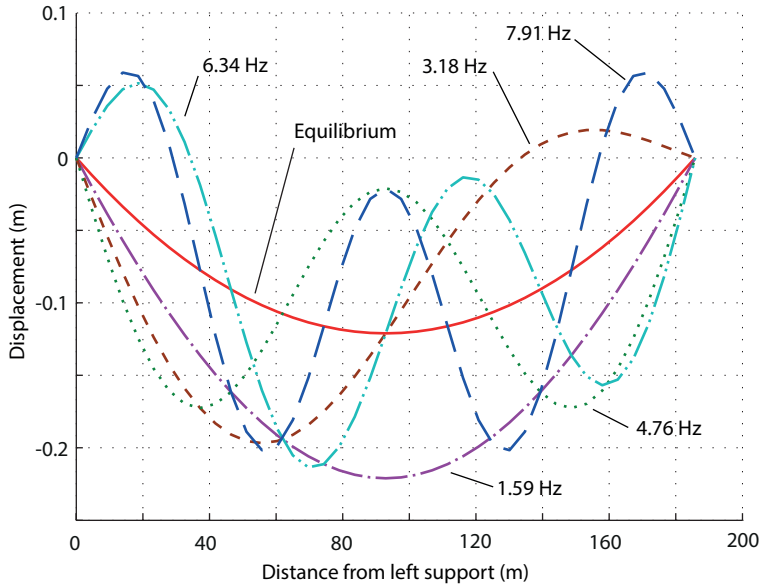

Figure 5.: *Vertical (in-plane) eigenmodes for a cable with the characteristics shown in Table 1.*

Table 2.: *Nature of various modes together with participation factors for a longitudinal translation of one end point. Same example as in Fig. 5.*

Mode no	Type	Symmetry	Eigenfrequency (Hz)	Participation factor
1	Out-of-plane	Symmetrical	1.59	0
2	In-plane	Symmetrical	1.59	5.63
3	In-plane	Anti-symmetrical	3.18	0.4
4	Out-of-plane	Anti-symmetrical	3.18	0
5	Out-of-plane	Symmetrical	4.76	0
6	In-plane	Symmetrical	4.76	1.52
7	In-plane	Anti-symmetrical	6.34	0.83
8	Out-of-plane	Anti-symmetrical	6.34	0
9	Out-of-plane	Symmetrical	7.90	0
10	In-plane	Symmetrical	7.90	0.49
13	In-plane	Symmetrical	11.0	0.09
17	In-plane	Symmetrical	14.0	0.51
25	Axial	Symmetrical	18.9	5380
62	Axial	Anti-symmetrical	37.8	10700
81	Axial	Symmetrical	56.7	16000
82	Axial	Anti-symmetrical	75.4	21200
83	Axial	Symmetrical	94.1	26200

closed in both ends or of a fluid oscillating in a tube. From first-order physics, it is known that the speed of sound, v, in a suspended cable is

$$v = \sqrt{\frac{E}{\rho}}$$

For our example, the speed of sound is 4.03×10^3 m/s. With the end nodes constrained there will be resonance, when the period of the oscillation equals the time it takes for the sound to go from one end of the cable to the other end and then be reflected back to first end. Considering also higher-order harmonics, the theoretical eigenfrequencies for axial vibrations then are multipla of the lowest axial eigenfrequency ν:

$$\nu = \frac{v}{2l}$$

For our example, Table 3 lists the axial eigenfrequencies as determined by the finite element model described above and the speed of sound. There is good agreement, in particular for the lower eigenfrequencies shown here, which are the ones of interest.

Table 3.: *Comparison of axial mode eigenfrequencies determined by the finite element model and from speed of sound.*

Mode no	Eigenfrequency from FE model (Hz)	Eigenfrequency from speed of sound (Hz)
25	18.9	18.8
62	37.8	37.6
81	56.7	56.4
82	75.4	75.2
83	94.1	94.0

Irvine (1999) has given an analytical approach for determination of eigenfrequencies of a suspended, taut cable. Normalized natural eigenfrequencies, ω', for symmetrical in-plane eigenmodes can be found as solutions to the transcendental equation

$$\tan\frac{\omega'}{2} = \frac{\omega'}{2} - \frac{4}{\gamma^2}\left(\frac{\omega'}{2}\right)^3 \tag{3}$$

The parameter γ^2 is

$$\gamma^2 = \frac{(\rho A g \cos\theta)^2 l^3 E A}{F^3 L_e}$$

where the symbols are defined in Table 1 and the parameter, L_e, is

$$L_e \approx l\left(1 + 8\left(\frac{\delta_{l/2}}{l}\right)^2\right) ,$$

where $\delta_{l/2}$ is the sag at the middle of the cable. For taut cables, $L_e \approx l$.

There are infinitely many solutions to (3) but for our purpose usually only few eigenmodes are of interest. The unnormalized natural eigenfrequencies can be found from

$$\omega = \omega' \sqrt{F/(\rho A)}/l$$

Solving the above transcendental equation iteratively for our example gives the eigenfrequencies shown in Table 4. There is fine agreement with the results from our finite element model, confirming the validity of the model.

Table 4.: *Comparison of symmetrical in-plane eigenfrequencies determined by the finite element model and from Irvine's analytical model.*

Mode no	Eigenfrequency from FE model (Hz)	Eigenfrequency from Irvine's model (Hz)
2	1.5913	1.5860
6	4.7634	4.7572
10	7.9064	7.9286

The analysis presented above is valid for fixed end points. In practice, one or both end points will be moved during operation. Since the mass of the cable near the end point is small compared to that of the attached parts, and since the rotation angle of winches can be servo-controlled with high bandwidth and stiffness, we can take the position of the end points as controlled input variables, and we are then interested in the cable forces at the end points. To deal with this, and for a moment ignoring damping, we rewrite (2):

$$\mathbf{M}\Delta\ddot{\mathbf{u}} + \mathbf{K}\Delta\mathbf{u} = \Delta\mathbf{f}$$

This is the equation for the full system (including end points). For numerical convenience, we now assume that the degrees of freedom have been resorted, so that the first three components of $\Delta\mathbf{u}$ are those of end point 1 ($(\Delta x_1, \Delta y_1, \Delta z_1)$) and the subsequent three components are those of end point 2 ($(\Delta x_{\mathrm{n_e}+1}, \Delta y_{\mathrm{n_e}+1}, \Delta z_{\mathrm{n_e}+1})$), and the remaining unsorted degrees of freedom are for the inner nodes of the cable. This involves switching columns and rows of $\mathbf{M}$ and $\mathbf{K}$ appropriately. We rewrite this equation on the form

$$\begin{bmatrix} \mathbf{M_{11}} & \mathbf{M_{12}} \\ \mathbf{M_{21}} & \mathbf{M_{22}} \end{bmatrix} \begin{Bmatrix} \Delta\ddot{\mathbf{u}}_1 \\ \Delta\ddot{\mathbf{u}}_2 \end{Bmatrix} + \begin{bmatrix} \mathbf{K_{11}} & \mathbf{K_{12}} \\ \mathbf{K_{21}} & \mathbf{K_{22}} \end{bmatrix} \begin{Bmatrix} \Delta\mathbf{u_1} \\ \Delta\mathbf{u_2} \end{Bmatrix} = \begin{Bmatrix} \Delta\mathbf{f_1} \\ \Delta\mathbf{f_2} \end{Bmatrix}$$

where $\mathbf{M_{22}}$ in fact is identical to the previously defined $\mathbf{M}'$, $\mathbf{K_{22}}$ is identical to to $\mathbf{K}'$, and $\Delta\mathbf{u_2}$ identical to $\Delta\mathbf{u}'$. Due to the above assumption, to ignore the influence of end cable mass on the motion of the end points, we let $\mathbf{M_{11}} \approx \mathbf{0}$. Since $\mathbf{M}$ is diagonal, then $\mathbf{M_{12}}$ and $\mathbf{M_{21}}$ are also null matrices. Hence the above equation becomes

$$\mathbf{K}_{11}\Delta\mathbf{u}_1 + \mathbf{K}_{12}\Delta\mathbf{u}' = \Delta\mathbf{f_1} \tag{4}$$

$$\mathbf{M}'\Delta\ddot{\mathbf{u}}' + \mathbf{K}'\Delta\mathbf{u}' = -\mathbf{K}_{21}\Delta\mathbf{u_1} \tag{5}$$

Since we merely wish to study the influence of end point movements, we have here for simplicity assumed that there are no external forces on the cable in addition

to those at the end points. Hence $\Delta\mathbf{f_2} = \mathbf{0}$ and $\Delta\mathbf{f_1}$ is equal to the forces at the end points. Then $\Delta\mathbf{u_1}$ is known, whereas $\Delta\mathbf{f_1}$ and $\Delta\mathbf{u}'$ are unknown. We can study the influence of end point movements by solving the equations for the end-constrained case with a load vector equal to $-\mathbf{K_{21}}\Delta\mathbf{u_1}$. Subsequently, the end point forces can be found from (4).

4.2 State-space Model

The above model is a second-order linear model. To fully exploit the many useful control engineering tools, we convert the model to a first-order state-space model on the usual ABCD form:

$$\dot{\mathbf{v}} = \mathbf{A}\mathbf{v} + \mathbf{B}\mathbf{w}$$
$$\mathbf{y} = \mathbf{C}\mathbf{v} + \mathbf{D}\mathbf{w}$$

where $\mathbf{A}$ is the *system matrix*, $\mathbf{B}$ the *input matrix*, $\mathbf{C}$ the *output matrix*, $\mathbf{D}$ the *feed-through matrix*, $\mathbf{v}$ is a state-space vector, $\mathbf{w}$ an input vector, and $\mathbf{y}$ an output vector. To determine the ABCD matrices, we first need to mass-normalize the eigenvectors. If $\boldsymbol{\psi}$ is an eigenvector, then the product of $\boldsymbol{\psi}$ and a constant will also be an eigenvector. We choose the constant for each eigenvector as described in Andersen & Enmark (2011) such that ${\boldsymbol{\Psi}'}_{\mathrm{m}}^{T}\mathbf{M}'\boldsymbol{\Psi}'_{\mathrm{m}} = \mathbf{I}$, where $\boldsymbol{\Psi}'_{\mathrm{m}}$ then is the eigenvector matrix holding the mass-normalized eigenvectors. Further using the methods presented in Andersen & Enmark (2011), we convert the second-order model derived above to ABCD form:

$$\mathbf{A} = \begin{bmatrix} \mathbf{0} & \mathbf{I} \\ -(\boldsymbol{\Omega}')^2 & -2\mathbf{Z}\boldsymbol{\Omega}' \end{bmatrix}$$
$$\mathbf{B}_{\mathrm{ends}} = -\begin{bmatrix} \mathbf{0} \\ {\boldsymbol{\Psi}'}_{\mathrm{m}}^{T} \end{bmatrix} \mathbf{K_{21}}$$
$$\mathbf{B}_{\mathrm{wind}} = \begin{bmatrix} \mathbf{0} \\ {\boldsymbol{\Psi}'}_{\mathrm{m}}^{T} \end{bmatrix}$$
$$\mathbf{C}_{\mathrm{ends}} = \mathbf{K_{12}} \begin{bmatrix} \boldsymbol{\Psi}'_{\mathrm{m}} & \mathbf{0} \end{bmatrix}$$
$$\mathbf{D}_{\mathrm{ends}} = \mathbf{K_{11}}$$

The matrix $\mathbf{B}_{\mathrm{ends}}$ relates to an input originating from a translation along either of the six degrees of the end points and the matrix $\mathbf{B}_{\mathrm{wind}}$ deals with a force input in three degrees of freedom for each of the internal nodes of the cable. The matrix $\mathbf{Z}$ is a diagonal matrix holding the assumed damping ratios for each of the modal coordinates.

This first-order model has twice as many degrees of freedom as the original second-order model. It is possible to perform a model reduction by disregarding those degrees of freedom that are outside the frequency range of interest. This is done by including only modes up to a certain order. In addition, eigenmodes that are known not to play a role, such as out-of-plane modes and anti-symmetrical in-plane modes, can be omitted. The eigenvector matrix then becomes rectangular with as many columns as there are eigenmodes retained and $\mathbf{A}$ becomes quadratic with as many rows and columns as there are eigenmodes retained. A substantial order reduction is then achieved.

The ABCD model is a useful building block in any simulation model involving control of a suspended object. Several such blocks can be combined into a large simulation model combining the dynamics of the individual cables and the suspended object.

Using the above model, we can determine *participation factors* as described in Andersen & Enmark (2011). For each mode, the value of the participation factor is a measure of the involvement of the mode when excited by a given input. For instance, the participation factors due to an excitation of the first degree of freedom of the second end point of the cable will be

$$\boldsymbol{\xi} = \boldsymbol{\Psi}'^{T}_{\mathrm{m}} \mathbf{K_{21}} \left\{ \begin{array}{cccccc} 0 & 0 & 0 & 1 & 0 & 0 \end{array} \right\}^{\mathbf{T}}$$

A value near zero of a participation factor signifies that the corresponding mode is poorly excited, whereas a numerically large value means that the mode is strongly excited. Table 2 shows participation factors for some of the more important modes of the cable of our example for an axial movement of an end point. The symmetrical low-order in-plane modes and the axial modes dominate when excited by a horizontal movement of the end point. Out-of-plane modes and anti-symmetrical modes are less important and can, in general, be disregarded in the model.

Using the state-space model, it is straightforward to determine frequency responses illustrating cable performance (Andersen & Enmark 2011). From a scalar input, w, to a scalar output, y, of the state-space model, the frequency response is

$$G(s) = \frac{y(s)}{w(s)} = \mathbf{C}\left(\mathbf{sI} - \mathbf{A}\right)^{-\mathbf{1}}\mathbf{B} + \mathbf{D} \tag{6}$$

where $\mathbf{C}$ for the single-input-single-output case has only one row, $\mathbf{B}$ only one column, and $\mathbf{D}$ only one column and row (scalar). The expression can be evaluated by setting the Laplace operator s to $\mathrm{i}\omega$, where ω is the angular frequency. This involves solving a set of linear equations for every frequency at which the frequency response is evaluated. We shall use this expression below.

5. Wind Load

Wind will act on the cable/gondola system in two ways, on the gondola and on the suspension cables. To study the wind load on the gondola, outset may be taken in a wind velocity spectrum. We choose a von Karman spectrum (Andersen & Enmark 2011):

$$S(\nu) = \sigma_v^2 \times \frac{4L_{\mathrm{v}}}{\bar{v}} \times \frac{1}{\left(1 + 70.7\left(\nu L_{\mathrm{v}}/\bar{v}\right)^2\right)^{5/6}} ,$$

where L_{v} is the *integral scale of turbulence* for longitudinal fluctuations (sometimes also called the outer scale of turbulence), $\bar{v}$ the mean air velocity, ν the frequency, and σ_v^2 the turbulence variance. The integral scale of turbulence sets the corner frequency between the Kolmogorov drop-off and the flat part of the spectrum.

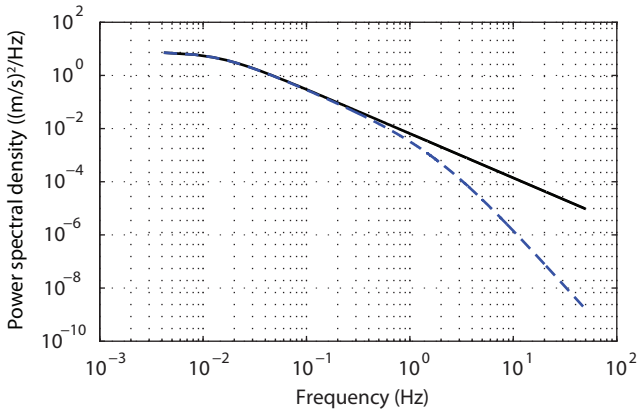

Figure 6.: *Wind velocity power spectral density with values applied for the example. The solid curve does not include cutoff due to high-frequency spatial filtering but the dashed curve does.*

Figure 6 shows the spectrum for the typical values $\bar{v} = 3$ m/s and $L_\mathrm{v} = 25$ m. The dashed curve includes a weighting factor to account for the high-frequency drop due to lack of coherence over the gondola:

$$\chi = \frac{1}{1 + \left(\frac{\nu}{\nu_\mathrm{c}}\right)^{4/3}} \tag{7}$$

where

$$\nu_\mathrm{c} = \frac{\bar{v}}{2l_\mathrm{s}} \approx \frac{\bar{v}}{2\sqrt{A_\mathrm{c}}} \,,$$

where $\bar{v}$ as before is the mean velocity, l_s is a characteristic gondola dimension and A_c a representative cross sectional area of the gondola. For our example, we used $A_\mathrm{c} = 0.6$ m^2.

The wind force power spectrum can be determined from the wind velocity spectrum (Andersen & Enmark 2011)

$$S_{force}(\nu) = C_\mathrm{d} \left(\rho_\mathrm{air} \bar{v}\right)^2 S(\nu) \,.$$

where C_d is the drag coefficient of the gondola and ρ_air the air density.

The power spectral density of the gondola excursion due to wind load can then be determined from

$$S_\mathrm{disp}(\nu) = |F(\nu)|^2 \, S_\mathrm{force}(\nu)$$

where $F(\nu)$ is the frequency response from gondola wind force to gondola displacement. The variance can be found as the area under the power spectral density curve.

There is also a wind load on the cables, potentially exciting in-plane eigenmodes by local, dynamical airflow in vertical direction with eddy sizes in the range 6-30 m. Also, the wind flow may generate flutter by vortex shedding, which will be in the range 100-600 Hz. Due to lack of spatial coherence and the filtering effect of the cable, this will only be an issue near the gondola. This effect has so far not been studied in detail.

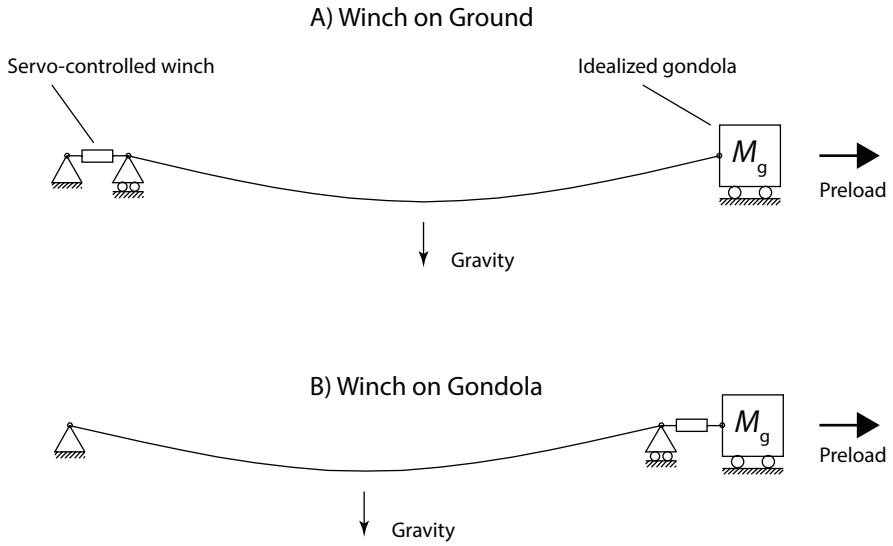

Figure 7.: *Generic gondola suspension model with only one cable to study the influence of design parameters.*

6. Design Parameter Selection

6.1 Generic Gondola Suspension Model

We now study the influence of various design parameters when using one or more cables for position control of a gondola. To do so, as an abstraction, we assume that the gondola is suspended by a single horizontal cable as shown in A) of Fig. 7. For our example, the gondola mass is taken to be 50 kg and the preload as before 1344 N. The mathematical model is then equal to the state-space model of the cable with the addition of two states for velocity and position of horizontal gondola translation. The frequency response from a horizontal displacement of the left end of the cable to the horizontal position of the gondola for our example can be determined using (6) and is shown in A) of Fig. 8. We have here assumed a damping ratio of 1 percent (although this is merely a rough estimate (Yamaguchi & Jayawardena 1992).

With position feedback from the gondola, it is possible to suppress wind disturbances with a winch control loop that controls the position of the left cable end as shown in the block diagram of Fig. 9. The controller applied for our example is a pure integrator with the addition of a pole/zero notch filter to reduce the influence of the first eigenmode of the gondola suspension. The pole is adjusted to match the first eigenfrequency of the gondola suspension with a damping ratio of 0.05, and the zero is placed at 10 Hz with a damping ratio of 1. It is not possible entirely to cancel the influence of the first eigenmode, so the bandwidth achievable for the closed-loop system will be less than the first eigenfrequency of the gondola suspension system and generally in the range 0.1–1 Hz depending on the choice of various design parameters.

We now turn to a study of the choice of various design parameters using the model and example just described.

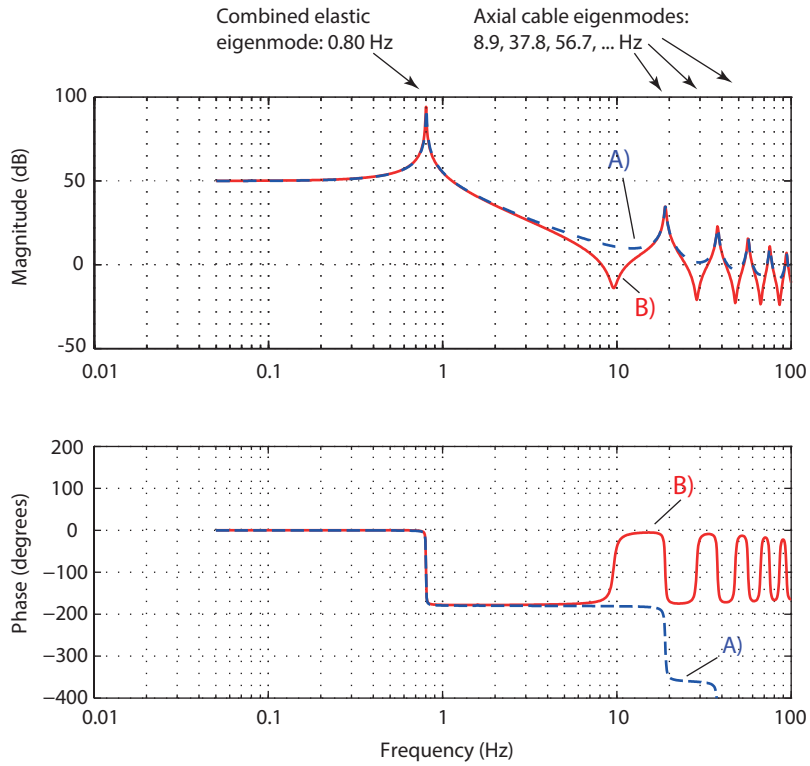

Figure 8.: *Frequency responses for the example introduced in Sect. 3.2. The curve A) takes a displacement of the left cable end as input and displacement of the gondola as output, whereas the curve B) is valid when the winch is placed on the gondola, i.e. with a displacement of the right cable end relative to the gondola.*

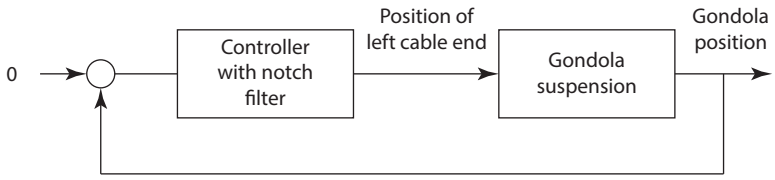

Figure 9.: *Block diagram for the winch control loop described in the text for the example introduced in Sect. 3.2.*

6.2 Influence of Modulus of Elasticity

We first study the influence of the cable E-modulus on performance. The E-modulus of the cable depends on the choice of material, and materials with a high E-modulus are generally more expensive than those with a lower value. It is obvious at the outset that the eigenfrequencies are important for servo control of the position of a gondola. For our example, Table 5 shows the influence of the E-modulus on the important eigenfrequencies for three different cables with the same preload but with different E-moduli. Also shown are the static stiffness values of the gondola suspension and the lowest gondola suspension eigenfrequencies.

From Table 5 it is apparent that the E-modulus of the cable should be as high as possible.

Table 5.: *Influence of E-modulus on performance. Same preload for all cases (1344 N).*

Modulus of elasticity	(GPa)	70	23.4	7
Cable eigenfrequency of mode 2	(Hz)	1.59	1.60	1.64
Cable eigenfrequency of mode 6	(Hz)	4.76	4.80	4.91
Cable eigenfrequency of mode 10	(Hz)	7.90	7.96	8.15
Cable eigenfrequency of mode 25	(Hz)	18.9	11.1	6.37
Cable eigenfrequency of mode 62	(Hz)	37.8	22.2	12.7
Static stiffness	(N/m)	1024	346	109
Sag	(m)	0.121	0.119	0.114
Lowest gondola eigenfrequency	(Hz)	0.72	0.42	0.24
Excursion of gondola, RMS	(mm)[1]	18	63	196

[1] with wind load and closed-loop control of a 50 kg gondola

6.3 Choice of Preload

It is also of interest to study the influence of cable preload on performance. Obviously, cable sag depends on the preload, leading to a dependence of the geometric stiffness on preload.

As can be seen in Table 6, use of a too small preload is unattractive because of the drastic decrease in static stiffness of the gondola suspension and low eigenfrequencies. However, above a certain limit, the influence of the preload is marginal because the elastic stiffness dominates over the geometric stiffness.

6.4 Influence of Cable Density

Tables 7 and 8 show the influence of cable density on cable performance for our generic suspension model with some representative preloads. As long as the preload is sufficiently high, the density is not a design driver.

6.5 Choice of Material

Table 9 lists characteristics of some typical cable materials. With the previous results in mind, we conclude that either an aramid (such as "Kevlar") or regular

Table 6.: *Influence of preload.*

Cable preload (N)	Length of unstressed cable (m)	Cable sag at equilibrium (m)	Static Stiffness at end (N/m)	Lowest in-plane cable eigenfrequency (Hz)	Lowest gondola eigenfrequency (Hz)
24200	183.195	0.601	9287	2.26	2.17
12100	184.488	0.121	9219	1.59	2.16
6056	185.142	0.243	9166	1.13	2.15
1363	185.668	1.081	7480	0.59	1.95
933	185.734	1.580	5380	0.57	1.65
361	186.000	4.088	698	0.55	0.59

Table 7.: *Influence of cable density. Case 1: High preload.*

Density	(kg/m^3)	1440	7800
Preload	(N)	673	614
Sag	(m)	0.243	1.271
Lowest cable eigenfrequency	(Hz)	1.13	0.51
Static stiffness at end	(N/m)	1019	956
Lowest gondola eigenfrequency	(Hz)	0.72	0.71

Table 8.: *Influence of cable density. Case 2: Low preload.*

Density	(kg/m^3)	1440	7800
Preload	(N)	40	174
Sag	(m)	0.851	5.09
Lowest cable eigenfrequency	(Hz)	0.55	0.49
Static stiffness at end	(N/m)	77.6	191
Lowest gondola eigenfrequency	(Hz)	0.49	0.31

(galvanized) steel can be applied. Polyester and polyamid, which are widespread rope materials, are not suitable for our application.

Table 9.: *Choice of material.*

Material	Tensile strength (MPa)	Density (kg/m^3	E-modulus (GPa)
Polypropylene	60	930	5
Polyester (Dacron)	1150	910	15
Polyamid (Nylon)	1000	1140	4
Aramid (Kevlar)	3000-3500	1440	70-140
Steel	1500-2000	7800	210
Stainless steel (Inox)	500-1000	7850	200

6.6 Choice of Cable Diameter

Table 10 shows performance characteristics for our generic example for four different choices of cable diameter and some representative preloads. Obviously, there is a higher wind drag for a thick cable than for a thin cable. Also, the static gondola suspension stiffness depends on the cable diameter, and the excursions of the gondola due to wind become much higher with a thin cable than with a thick cable. Hence, the cable should be chosen as thick as possible taking into account practical aspects, such as the need for more robust adjoining structures with a thick cable and a high preload.

Table 10.: *Choice of cable diameter.*

Cable diameter (mm)	Cable mass (kg)	Typical preload (N)	Static stiffness 6 m/s (N/m)	RMS gondola velocity[1] (mm/s)	RMS gondola excursion[1] (mm)
1.85	0.72	1340	1020	87.5	19.6
3.70	2.88	5380	4100	22.3	2.60
5.55	6.47	12100	9200	9.4	0.73
7.40	11.5	21508	16400	5.3	0.31

[1] Due to wind at 6 m/s acting on gondola and closed-loop position control with winch.

6.7 Location of winch

The winch may be placed on the gondola instead of on the ground as shown in the generic model B) of Fig. 7. The corresponding frequency response from winch position to gondola position is shown in curve B) of Fig. 8. It is equally difficult to stabilize a control system with the winch located on the ground and on the gondola, so there is no real advantage of moving the winch to the gondola.

In addition to the approaches for gondola stabilization studied here, a fast beam steering mirror will be needed to compensate for gondola vibration. This possibility has not yet been studied in detail.

7. Discussion

We have set up a linear cable model using a non-linear finite element approach. Model performance agrees well with existing analytical approaches and with speed-of-sound considerations. Also, there is good agreement with the purely analytical model formulated in our previous publication (Enmark et al. 2011). The present model is however preferable due to its simplicity.

Using a cable example with a generic suspension model, we have studied the influence of design parameter selection. We conclude that the preload should be sufficiently high to ensure that the axial elasticity of the cable dominates over the geometrical elasticity. From wind considerations, we find that the wind load on the gondola dominates over wind load on the cable, although vortex shedding (flutter) may be an issue near the gondola.

Aramid and steel are suitable cable materials. The cable diameters should be as large as practically possible.

Gondola motion faster than about 1/2 fringe per millisecond cannot be detected and taken into account with a fast camera working at 1 kHz. This corresponds to 0.5-1 μm/ms in the near infrared. Although we here use a simple, very generic model, the results of Table 10 tend to suggest that the gondola velocity is too high even for short exposures (> 5.3 μ/ms), which could explain why no stellar fringes have been detected at the Haute-Provence observatory test site (Dejonghe et al. 2014). A closer study with a full model of all cables is on the way to establish whether this is indeed the case.

Finally, it is apparent that gondola velocity and excursions due to wind are far too high for long exposures without additional corrections, such as tip/tilt beam steering, fringe tracking, etc. It is believed that a much better gondola stability can be obtained using servo-controlled reaction wheels and reaction masses on board the gondola with appropriate angular and linear gondola acceleration, velocity and position feedback. Gyros and accelerometers may be needed. A further study of this possibility is planned.

References

Kamran Ahmadi-Kashani 1983, Development of cable elements and their applications in the analysis of cable structures. PhD thesis, Division of Structural Engineering, Department of Civil and Structural Engineering, University of Manchester, Institute of Science and Technology.

Torben Andersen and Anita Enmark 2011, Integrated Modeling of Telescopes, Springer.

H. Le Coroller, J. Dejonghe, et al. 2012, "Tests with a Carlina-type Diluted Telescope. Primary Coherencing", A&A, vol. 539, no. A59, 17pp.

J. Dejonghe et al. 2014, "The Carlina Diluted Telescope: A new class of interferometer. Opto-mechanical design and results of the OHP experiment", in Proceedings of Haute Provence Observatory Colloquium (23-27 September 2013), L. Arnold, H. Le Coroller, and J. Surdej, eds.

Y. M. Desai, N. Pipplewell, A. H. Shah, and D. N. Buragohain 1988, "Geometric nonlinear static analysis of cable supported structures", Computers & Structures, vol. 29, no. 6, pp. 1001-1009.

A. Enmark, T. Andersen, M. Owner-Petersen, R. Chakraborty, and A. Labeyrie 2011, "Integrated model of the Carlina Telescope", in Integrated Modeling of Complex Optomechanical Systems, vol. 8336, pp. 83360J-83360J-14.

M.I. Gambhir and Barrington de V. Batchelor 1977, "A finite element for 3-D prestressed cablenets", International Journal for Numerical Methods in Engineering, vol. 11, pp. 1699-1718.

W. M. Henghold and J. J. Russell 1976, "Equilibrium and natural frequencies of cable structures (a nonlinear finite element approach)", Computers & Structures, vol. 6, pp. 267-271.

H. Max Irvine 1981, Cable Structures, The MIT Press.

H. B. Jayaraman and W. C. Knudson 1981, "A curved element for the analysis of cable structures", Computers & Structures, vol. 14, no. 3-4, pp. 325-333.

Robert Levy and William R. Spillers 2003, Analysis of Geometrically Nonlinear Structures. Kluwer Academic Publishers, 2nd ed.

Haluk Ozdemir 1979, "A finite element approach for cable problems", International Journal of Solids and Structures, vol. 15, pp. 427-437.

Wei-Xin Ren, Meng-Gang Huang, and Wei-Hua Hu 2008, "A parabolic cable element for static analysis of cable structures", International Journal for Computer-Aided Engineering and Software, vol. 25, no. 4, pp. 366-384.

H.-J. Schek 1974, "The force density method for form finding and computation of general networks", Computer Methods in Applied Mechanics and Engineering, vol. 3, pp. 115-134.

U. Starossek 1994, "Cable Dynamics - A Review", Structural Engineering International, vol. 3, pp. 171-176.

Ivar Talvik 2001, "Finite element modelling of cable networks with flexible supports", Computers & Structures, vol. 79, pp. 2443-2450.

Gunnar Tibert 1999, Numerical Analyses of Cable Roof Structures. TRITA-BKN Bulletin 46, Kungl. Tekniska Hoögskolan, Institionen för Byggkonstruktion.

Hirold Yamaguchi and Loranjana Jayawardena 1992, "Analytical estimation of structural damping in cable structures", Journal of Wind Engineering and Industrial Aerodynamics, vol. 41-44, pp. 1961-1972.